Journal of Marine Research, 53, 739–770, 1995

Structure of an inertial deep western boundary current

by Robert S. Pickart[1] and Rui Xin Huang[1]

ABSTRACT

An inertial model of the deep western boundary current (DWBC) is presented where the cross-stream distribution of potential vorticity varies in a realistic fashion. The case of uniform potential vorticity, which has been solved earlier, is included for comparison. The potential vorticity distribution used in the model is obtained from a hydrographic density section across the North Atlantic DWBC. The model solutions using this distribution differ significantly from the uniform potential vorticity case. Most notably the current is wider and weaker with substantially reduced relative vorticity, more indicative of observed DWBCs. The addition of an exponential continental slope leads to a further constraint on the existence of the current. Finally, it is demonstrated how a topographic ridge can partially block the DWBC and give rise to recirculation of the deepest water, reminiscent of the deep flow near the Southeast Newfoundland Rise in the North Atlantic.

1. Introduction

There have been relatively few attempts to examine the structure of deep western boundary currents (DWBCs), which are a crucial element of the ocean's meridional circulation. This is partially due to a deficiency in the observational description of such currents compared to the upper ocean circulation. In light of an increased effort to determine the ocean's role in climate change, it is especially important to obtain a better understanding of the basic dynamics of DWBCs. Transporting water which has been recently convected from the surface, DWBCs ventilate the deep basin interiors and are the initial mechanism through which the abyssal ocean responds to variations in climate. To sort out the complex role of DWBCs in this ventilation process we need first to clarify the dynamics of the mean currents. This in turn will aid the investigation of their variability and response to variable forcing.

The modeling work to date on DWBCs can be divided into several fairly distinct categories. The earliest approach (which is still used successfully today) was a streamtube formulation whereby the properties of the DWBC are averaged across-stream; thus the current is solely a function of downstream distance from its origin. Smith (1975) successfully modeled the downstream evolution of the Denmark Strait overflow in this fashion, explaining the role of friction in allowing the current to

1. Woods Hole Oceanographic Institution, Woods Hole, Massachusetts, 02543, U.S.A.

descend the continental slope as well as the role of entrainment in altering the current's properties. Speer and Tziperman (1990) also used this approach in their combined model of a deep boundary current and associated interior density structure.

In these models it is the initial evolution of the current which is studied as the DWBC descends from an overflow (though Speer and Tziperman (1990) included a detrainment team farther downstream). In each case a "far field" DWBC is reached in which the current equilibrates at a constant depth on the continental slope, with little further change. In reality, DWBCs can change significantly in this far field as they ventilate the interior basins. For example, Pickart (1992) has shown that the North Atlantic DWBC becomes significantly less dense and systematically shoals over a 2000 km distance downstream of the Grand Banks of Newfoundland. The need exists to investigate such downstream changes in the DWBC. Recently MacCready (1993) has taken this perspective in explaining why DWBCs are able to persist far from their source without spinning down.

Another approach to DWBC modeling has been an inertial formulation, which is the approach considered in this study. Stommel and Arons (1972) used an inverse reduced gravity model to investigate the effect of bottom slope on the width of DWBCs. They determined that a locally weaker bottom slope results in a wider DWBC, though they did not pursue the detailed structural evolution of the current. Johnson (1993) extended Stommel and Arons' (1972) formulation to consider how an inertial DWBC crosses the equator, and carefully examined the pronounced change in the current on the β-plane. Subsequent to the equatorward crossing, however, the solution becomes oscillatory and hence unrealistic.

A third class of DWBC models uses a linear formulation in which cross-stream diffusion of momentum and density are considered. Warren's (1976) model contained an outer geostrophic DWBC coupled to an inner Munk-layer flow. The outer current contained realistic features of observed mid-latitude DWBCs, including the cross-stream scale of the flow. Pedlosky and Chapman's (1993) model of the abyssal circulation also contains this type of boundary layer flow, modified by the presence of a broad meridional bottom slope. Zonal variation in topography is not considered in either of these models.

A fourth class of problems has addressed DWBCs within the context of basin-wide general circulation, which ties together the adjoining interior flow field. The approach here is often through numerical simulation. A hierarchy of such models has investigated the spin-up and general behavior of abyssal flow in the presence of significant bottom topography (see Straub *et al.,* 1993; Kawase and Straub, 1991; and Kawase, 1993). The latter study investigates the transposition of the Antarctic bottom water to the eastern boundary due to the effect of topographic beta in the tropical North Atlantic. Recent work has also addressed the stability of DWBCs and their effect on the adjacent interior flow. Spall (1994) reveals that an unstable

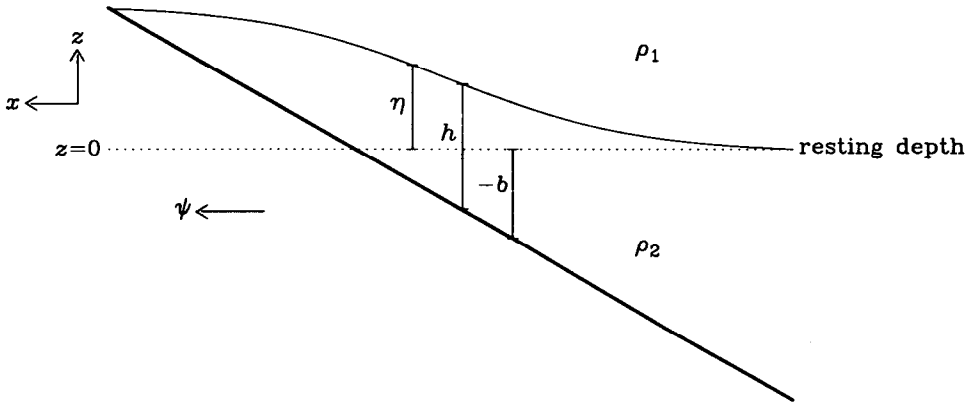

Figure 1. Schematic of the model DWBC. The moving lower layer has density ρ_2, while the resting, infinite upper layer has density ρ_1. The interface flattens out on both sides of the current corresponding to the motionless shoulders.

DWBC can radiate waves that drive a mean interior circulation, one which is fundamentally different than the Stommel-Arons deep flow pattern.

The purpose of this paper is to examine in simple fashion the alongstream evolution of DWBCs within an inertial framework. Frictional effects and entrainment are purposely not considered in order to explore thoroughly the basic inertial dynamics. We seek here to determine specifically whether a purely inertial model can result in realistic features of a DWBC over a large (basin-scale) length. Toward this end we examine both a uniform potential vorticity current—like that considered by Stommel and Arons (1972)—and a DWBC with a realistic cross-stream distribution of potential vorticity. Results are discussed in light of observations of the North Atlantic DWBC. Finally, the effect of varying topography is considered, with application to the Southeast Newfoundland Rise in the North Atlantic.

2. Formulation

An appropriate framework in which to study an inertial DWBC was developed by Stommel and Arons (1972) who analytically solved the case of a uniform potential vorticity current. Johnson (1993) extended this to the β-plane to study how the DWBC crosses the equator. We restrict ourselves here to mid-latitudes and adapt the same framework, though a solution is obtained by use of a streamfunction coordinate transformation which allows consideration of a more general distribution of potential vorticity.

A reduced gravity model is used which consists of a moving layer underneath a thick, stagnant layer (Fig. 1). The current is semi-geostrophic,

$$-fv = -g'\eta_x = -g'(h + b)_x, \tag{1}$$

$$uv_x + vv_y + fu = -g'\eta_y = -g'(h + b)_y, \tag{2}$$

$$(uh)_x + (vh)_y = 0, \tag{3}$$

where positive (x, u) are onshore, positive (y, v) are downstream (equatorward) and positive z is upward. The bottom depth relative to $z = 0$ is b and the layer thickness is h, thus the interface height is $\eta = (h + b)$ (Fig. 1). The reduced gravity is $g' = (\rho_2 - \rho_1/\rho_2)g$, and $f(y)$ is the Coriolis parameter. Using Eqs. (1)–(3) it is easily shown that

$$\boldsymbol{u} \cdot \nabla Q = 0, \tag{4}$$

$$\boldsymbol{u} \cdot \nabla B = 0, \tag{5}$$

where $Q = (f + v_x)/h$ is the potential vorticity, $B = v^2/2 + g'(h + b)$ is the Bernoulli function, and $\boldsymbol{u} = (u, v)$. This in turn implies that these quantities are functions only of the transport streamfunction ψ,

$$Q = Q(\psi); \quad B = B(\psi), \tag{6}$$

where

$$\psi_x = vh, \tag{7}$$

$$-\psi_y = uh. \tag{8}$$

Furthermore, the Bernoulli function and potential vorticity are related by,

$$B(\psi) = \int Q(\psi)\, d\psi. \tag{9}$$

Because of the sole dependence of these quantities on ψ in the inertial framework, it is natural to consider ψ as the independent variable. Using the transformation obtained from (7)

$$\frac{\partial}{\partial x} = \frac{\partial}{\partial \psi}\frac{\partial \psi}{\partial x} = vh\frac{\partial}{\partial \psi}, \tag{10}$$

the expressions for the potential vorticity and Bernoulli function can be re-cast as equations for downstream velocity and layer thickness,

$$v_\psi^2 = 2\left(Q(\psi) - \frac{f}{h}\right), \tag{11}$$

$$h = \frac{2\int Q(\psi)\, d\psi - v^2}{2g'} - b(x). \tag{12}$$

Note that the y-variation appears parametrically through the dependence of both f and $b(x)$ with latitude. The explicit dependence of x on ψ is given by the above

transformation,

$$x_\psi = \frac{1}{hv}, \tag{13}$$

thus (11)–(13) represent three equations for the three unknowns (h, v, x), to be solved successively at each latitude y.

3. Constant potential vorticity current

Stommel and Arons (1972) considered a DWBC with uniform potential vorticity, i.e. $Q(\psi)$ = constant. Since the alongstream evolution of such a mid-latitude DWBC was not investigated by these authors, it is considered here as the first case.

a. Scaling. It is useful to re-write Eqs. (11)–(13) using the following non-dimensional variables: $x = L_c x', h = Hh', f = f_o f', v = Vv', \psi = \Psi\psi'$, where the basic scales are:

$$L_c \sim 150 \text{ km},$$

$$H \sim 1500 \text{ m},$$

$$V = \frac{g'H}{f_o L} \sim 0.1 \text{ m/s},$$

$$\Psi = \frac{g'H^2}{f_o} \sim 20 \text{ Sv},$$

$$f_o = 1.2 \times 10^{-4}(55\text{N}),$$

$$g' = .001 \text{ m/s}^2.$$

We will vary the reduced gravity between .001–.005 m/s^2. The lower value is roughly that used by Johnson (1993). To get an idea of a representative g' for the North Atlantic DWBC, we assembled 80 historical hydrographic stations taken along the continental slope in the Mid-Atlantic Bight. The value of g' was computed at each station using an interface of σ_3 = 41.42 kg/m^3 (see Fig. 6), which corresponds to a depth of roughly 2000–2500 m. The resulting g' values were not very sensitive to the total depth of the station, which is not surprising since the isopycnals in the DWBC generally slope downward offshore. The computed values ranged between .002–.0045 m/s^2, with an average of .0031 m/s^2. This justifies our chosen range of g' for the model.

It is worth noting that a scaling argument can be used to estimate the importance of friction in the DWBC, which sheds light on our inertial approach. Following the

formulation of Killworth (1993), the modification of potential vorticity due to friction is

$$\boldsymbol{u} \cdot \nabla Q = -\frac{D_x}{h}, \tag{14}$$

where D represents dissipation. Using typical scales for the DWBC, we wish to demonstrate that the effect due to friction is minor and hence (14) reduces to (4) at leading order. Assuming without loss of generality that dissipation is in the form of lateral diffusion, a scale estimate of (14) results in

$$\frac{V\delta Q}{L_a} \sim -\frac{\kappa V}{L_c^3 H}, \tag{15}$$

where δQ represents the change in potential vorticity (due to friction) over the alongstream length scale L_a. Dividing both sides by the scale for potential vorticity, $Q \sim f_o/H$, gives an estimate of the percentage downstream change,

$$\frac{\delta Q}{Q} \sim \frac{\kappa L_a}{f_o L_c^3}. \tag{16}$$

Taking $\kappa = 10^7$ cm^2/s (a generous estimate for the deep water, e.g. Pickart and Hogg, 1989) and $L_a = 5000$ km implies that $\delta Q/Q \sim .01$; i.e. to leading order Q should be conserved in the DWBC and an inertial framework is justified. We also note that Spall's (1994) numerical study of DWBCs included bottom drag, lateral friction, and cross-isopycnal mixing, however the dominant balance was inertial. It is of course true that at low latitudes ($f \to 0$) frictional effects should become of leading order. As noted above, however, our model applies to mid-latitudes.

Following Stommel and Arons (1972) we consider a linearly sloping bottom $b(x) = \alpha x$ (no y-dependence), and set $Q(\psi) = f_o/H$. Substituting these into (11)–(13) and dropping the primes, we obtain the non-dimensional equations for the uniform potential vorticity current,

$$v_\psi^2 = \frac{2}{\epsilon}\left(\frac{h-f}{h}\right), \tag{17}$$

$$h = \psi - \frac{\epsilon}{2}v^2 - sx, \tag{18}$$

$$x_\psi = \frac{1}{hv}, \tag{19}$$

where $s = \alpha L_c/H$ is the non-dimensional bottom slope, $\epsilon = (L_D/L_c)^2$ the Burger number, and $L_D = (g'H)^{1/2}/f_o$ the internal deformation radius.

b. Method of solution. Stommel and Arons (1972) showed that there are two types of boundary conditions for the onshore side of the current: vanishing layer thickness or zero velocity. In the latter there is a stagnant region between the continental slope and edge of the DWBC (Fig. 1). Furthermore, the condition for the stagnant case is (dimensionally)

$$\alpha < \frac{f_o\sqrt{H}}{\sqrt{g'}} \approx .1, \tag{20}$$

for the above scales. For the North Atlantic DWBC the typical bottom slope is .01, so clearly the stagnant condition applies. The appropriate boundary condition for the onshore edge is thus

$$v = 0 \qquad \text{at } \psi = \psi_{\max}, \tag{21}$$

where $\psi_{\max}$ is the total volume flux of the DWBC (assumed constant with latitude). There is observational evidence to support the existence of such a stagnant region located onshore (e.g. Fig. 6). It should be noted, however, that at low latitudes the zero thickness boundary condition eventually takes over as the DWBC meets the continental slope and the above scales no longer apply (see Johnson, 1993). In our case this does not happen until about 10N which is taken as the southern limit of our domain. Johnson (1993) investigates the character of the current in the neighborhood of the equator.

The offshore side of the DWBC corresponds to $\psi = 0$. The associated boundary conditions are (Fig. 1)

$$x = x_o, v = 0, h = -sx_o(\eta = 0) \qquad \text{at } \psi = 0. \tag{22}$$

The latter condition on h sets the Bernoulli function equal to zero at the offshore edge of the DWBC (this specifies the integration constant in (9)). Note that specifying $v = 0$ at the offshore boundary seemingly suggests that x_ψ is initially infinite (by Eq. (19)), hence yielding an unbounded DWBC width. That this is not the case can be seen by re-casting the integral of (19) using Eq. (17),

$$x - x_o = \int_0^\psi \frac{d\psi}{hv} = \epsilon \int_0^v \frac{dv}{(h - f)}. \tag{23}$$

Since we require a southward flowing boundary current this means initially $v_x > 0$, or by (10) $v_\psi^2 > 0$. Hence by (17) $h > f$ at the offshore boundary, which ensures that the integral (23) is indeed finite at the boundary. Note that dimensionally this condition on layer thickness simply states that for $Q = (f + v_x)/h$, h must be large enough at the offshore boundary so that v_x is initially positive.

The northern boundary of the model corresponds to a location well downstream of the northern overflow, i.e. downstream of the descending plume which at that point

is still strongly influenced by turbulent entrainment and friction. For the North Atlantic DWBC this might be after the current enters the Labrador Sea, say near 60N. As mentioned earlier, our approach is to solve for the cross-stream structure of the current successively at each latitude over the length of the domain. At each latitude the solution is obtained as follows. Since x is a dependent variable, the location and width of the DWBC are unknown beforehand; these depend on the choice of transport. The solution is initiated at $\psi = 0$ (the eastern edge of the current where $v = 0$) proceeding onshore toward larger positive ψ. As the rhs of (17) must be initially positive to ensure a southward flowing boundary current, inserting the initial value of h gives $|x_o| > f/s$ which provides the onshore limit of the eastern edge of the DWBC (any shallower than this results in a layer thickness which is too small). Using this as a guide we guess a value of x_o, which specifies the initial conditions, then solve (17) as an ordinary differential equation for the next value of v. This is used to solve (19) in similar fashion for x, and finally (18) is evaluated for h. This process is repeated until the velocity decreases back to zero, which is the onshore edge of the current. The corresponding final value of ψ is the transport of the current which in general is not our desired value, ψ_{max}. Thus, x_o is revised and a new solution found. This process is iterated until the desired ψ_{max} is obtained. The accuracy of the solution can be checked by computing the cross-stream distribution of potential vorticity and verifying that it is indeed constant and equal to the specified value. All model solutions (in this section and subsequent sections) accurately reproduced the specified potential vorticity $Q(\psi)$.

c. Results. Just as there is an onshore limit for x_o (the eastern edge of the DWBC), an offshore limit exists beyond which the solution is unbounded. To understand this, consider that for the constant Q case, differentiating the expression for the potential vorticity gives

$$v_{xx} = \frac{f_o}{H}(h_x), \tag{24}$$

so that if h decreases initially then so will the shear v_x. Since $v = 0$ at the offshore boundary, (1) implies that initially $\eta_x = 0$ and $h_x = -b_x = -\alpha$. Thus the shear v_x does in fact decrease, and since it is initially positive for a southward flowing DWBC it will eventually pass through zero—corresponding to the peak velocity of the current. At this point the layer thickness is $h = (f/f_o)H$. Note that at the offshore edge of the current h_x is the same value $(= -\alpha)$ regardless of how far out the edge is, i.e. regardless of how large x_o is. So one can envision that if the edge is far enough offshore with a correspondingly large h, the layer thickness will not be able to decrease to the value $(f/f_o)H$ by the time v_x reaches zero. What happens in this case is that v_x and h reach a minimum value and then both begin to increase without bound, hence the unbounded solution (Fig. 2).

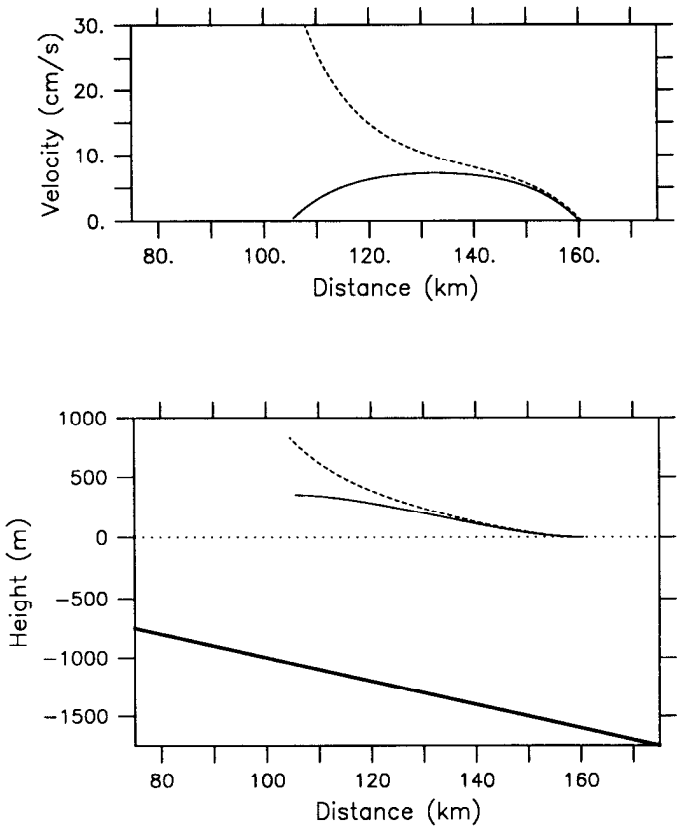

Figure 2. Two solutions for the uniform potential vorticity current. The upper panel is downstream velocity, and the lower panel is the interface height (light lines) and bottom (heavy line). The solid line shows the physical solution where h decreases onshore, while the dashed-line is the non-physical solution which increases without bound onshore. In this example the parameters are $g' = .001$, the bottom slope $\alpha = .01$, and the latitude = 55N.

An important observation to be made here is that only in this case (where h increases without bound) can the interface slope more steeply than the bottom. As seen in Figure 2, the physical (bounded) solution has $v_{xx} \leq 0$ everywhere which by (24) means $h_x \leq 0$; thus h must decrease and η cannot slope more steeply than the bottom. This condition is dependent in part on the offshore boundary condition ($v = 0$) in which the interface slope decreases to zero as the interface joins the stagnant interior (Fig. 1). We note that an offshore boundary condition of zero thickness is also possible. In that case the DWBC is an isolated lens of dense water situated on the continental slope (e.g. Griffiths *et al.* (1982); Nof and Olson (1993)), and the interface does slope more steeply than the bottom at the offshore edge. However, such a lens-like DWBC structure is found only in the first 500 km or so of

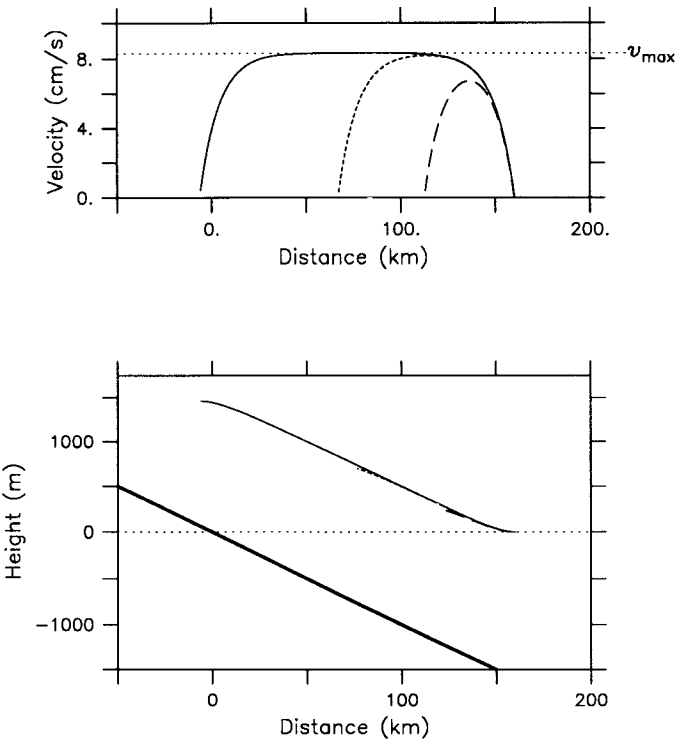

Figure 3. Three solutions of the uniform potential vorticity current with increasing transport. The upper panel is the downstream velocity with the maximum possible value indicated. The lower panel is the interface. The parameters are $g' = .001$, $\alpha = .01$, latitude = 55N.

the northern overflow (Grant, 1968); for the vast majority of the current the interface does indeed merge with the stagnant interior as we have modeled here.

The above limit on interface slope does not imply, however, that the transport of the current is limited. As x_o is chosen closer and closer to the critical value where the solution becomes unbounded, the width of the current (i.e. the onshore edge) becomes larger and larger while the velocity stays bounded: the peak of the current simply extends over an ever increasing region where $v_{x\alpha} = h_x = 0$ (Fig. 3). In this region the depth h maintains the constant value $(f/f_o)H$ and the interface parallels the bottom. Thus the maximum velocity which the DWBC can obtain is, from (1),

$$v_{\max} = (g'/f)b_x. \tag{25}$$

For the parameters in Figure 3 the maximum velocity given by $(g'/f)\alpha$ is 8.3 cm/s which is borne out by the graph.

The solution that we use for the example of a constant potential vorticity DWBC has a transport of 5 Sv, bottom slope of .01, and $g' = .001$ m/s^2. These are all

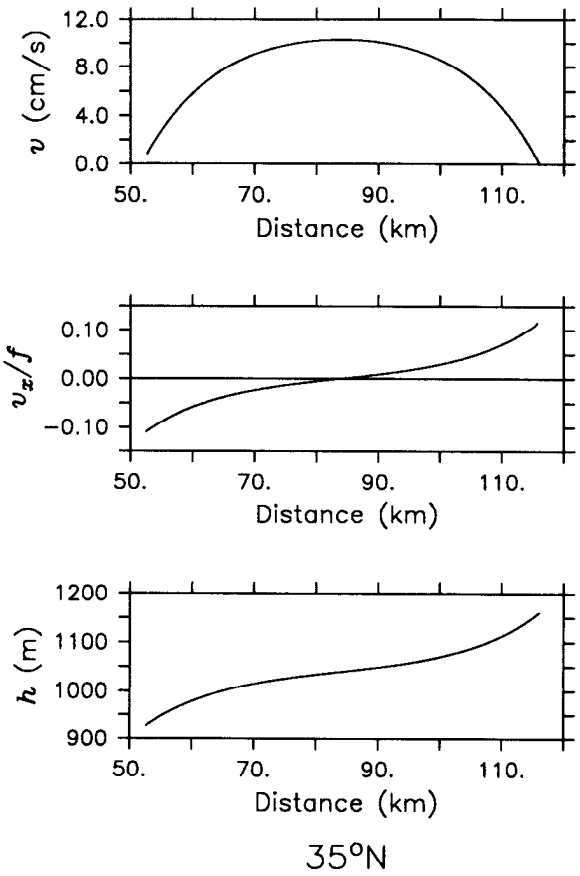

Figure 4. Cross-stream structure of the uniform potential vorticity current at 35N. The upper panel shows the downstream velocity, the middle panel shows the relative vorticity normalized by f, and the lower panel shows the layer thickness. The parameters are $g' = .001$, $\alpha = .01$, Transport = 5 Sv.

representative of the North Atlantic DWBC. The cross-stream structure of the current at 35N shows a peak velocity of 10 cm/s and variation in h of 250 m (Fig. 4). Note that the relative vorticity of the current reaches 10% of f at the edges of the current. The alongstream evolution of the current (Fig. 5) shows the excursion of the DWBC across the continental slope, a feature noted by Johnson (1993). This is simply the response of the current to decreasing f; i.e. by moving into shallower topography the layer thickness h can decrease in order to maintain a constant Q. Note in Figure 5b that the interface slope also decreases (and width increases) to the south in response to decreasing f. Interestingly, this causes the peak velocity of the current to fall farther below the maximum possible value (Fig. 5c). This suggests that as one progresses to the south there should be less tendency for the DWBC

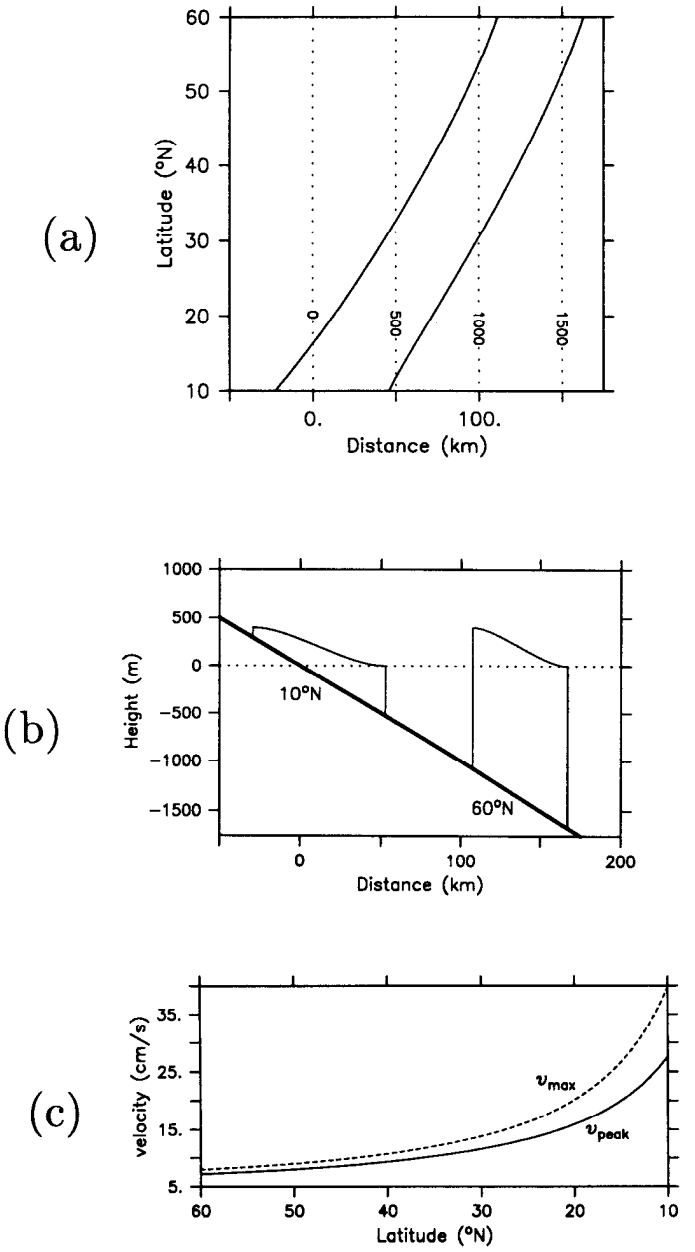

Figure 5. Alongstream evolution of the uniform potential vorticity current with parameters $g' = .001$, $\alpha = .01$, Transport = 5 Sv. (a) Alongstream path of the current; the topography is indicated by the dotted lines. (b) Cross-section of the interface revealing the change in structure from 60N to 10N. (c) Alongstream trend in peak velocity of the current, where the maximum possible value is indicated by the dashed line.

isotherms to parallel the bottom; there is in fact evidence of this in the observations (for example, compare typical mid-latitude sections to those occupied in the Labrador Sea as seen in Grant (1968)).

As the current reaches the tropics the value of the relative vorticity increases substantially, and for larger values of g' it becomes unrealistically large. This casts doubt on the appropriateness of the constant potential vorticity assumption. While the observations indicate an increased relative vorticity at these latitudes (e.g. Johns *et al.,* 1993), the values from the model are clearly too large. This, together with the small width of the current, is among the reasons for considering a more realistic cross-stream distribution of potential vorticity in the next section.

4. Realistic potential vorticity current

a. Determination of $Q(\psi)$. The use of ψ as the independent variable in the model governing equations (11)–(13) enables us to consider any distribution of potential vorticity $Q(\psi)$. We used a typical hydrographic density section of the North Atlantic DWBC (at 35N) to compute a realistic potential vorticity profile. Specifically, we used a smoothed density surface near 2500 m as the interface (Fig. 6) to obtain the equatorward geostrophic velocity according to (1). Then using the smoothed bottom topography we computed the cross-stream profile of transport and potential vorticity, which were used to obtain Q as a function of ψ (Fig. 6c). Note the shape of $Q(\psi)$ compared to the constant value of the last section, particularly the sharp increase in potential vorticity at the onshore edge of the current where the layer thickness decreases substantially.

For implementation purposes the Q profile determined from the data was approximated by a 4th-order polynomial (Fig. 6c)

$$Q(\psi) = \sum_{i=0}^{4} A_i \psi^i. \tag{26}$$

This expression was substituted into (11) and (12) and non-dimensionalized to give the following governing equations for the realistic potential vorticity current (analogous to Eqs. (17)–(19)),

$$v_\psi^2 = \frac{2}{\epsilon}\left(\frac{\left(\sum_{i=0}^{4} \tilde{A}_i \psi^i\right)h - f}{h}\right), \tag{27}$$

$$h = \sum_{i=0}^{4} \frac{\tilde{A}_i}{(i+1)} \psi^{i+1} - \frac{\epsilon}{2} v^2 - sx, \tag{28}$$

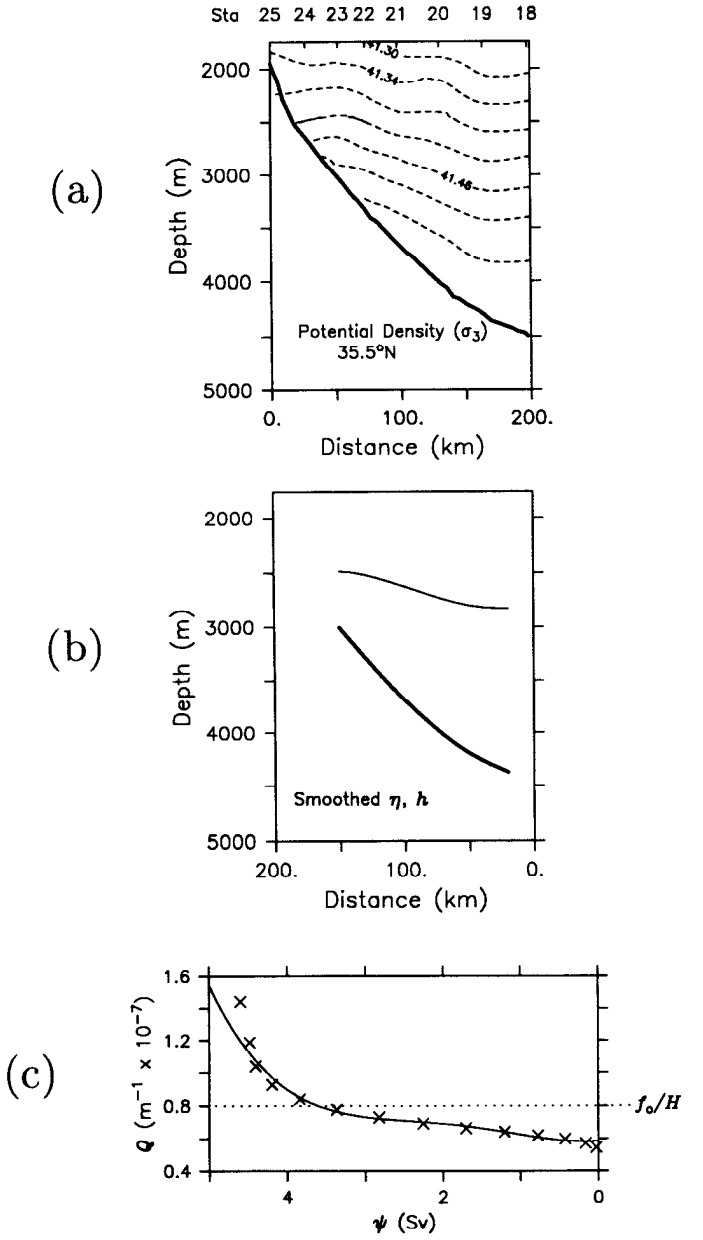

Figure 6. (a) Section of potential density referenced to 3000 db for the North Atlantic DWBC near 35N. (b) Low-pass of the density interface $\sigma_3 = 41.42$ from (a) (light solid line), and low-passed bottom topography from (a) (dark solid line). (c) Potential vorticity versus transport (x's) computed using the interface and bottom profiles in (b). The solid line is the polynomial fit used in the model (see text), where the coefficients are $A_0 = .5862$, $A_1 = -.0407$, $A_2 = .1314$, $A_3 = -.0592$, $A_4 = .0084$. Also shown is the constant value of potential vorticity for the uniform Q current (dashed line).

$$x_\psi = \frac{1}{hv}, \tag{29}$$

where

$$\tilde{A}_i = \frac{HA_i}{f_o}\left(\frac{g'H^2}{f_o}\right)^i.$$

The bottom slopes linearly as before (no y-dependence), and the boundary conditions remain the same as in the uniform potential vorticity case (21)–(22).

b. Results. In contrast to the case of uniform potential vorticity, there is a maximum transport solution for the realistic potential vorticity current. Recall that in the uniform Q case the onshore extent of the current was able to increase without bound and hence support ever increasing transport. In the present case as the transport increases so does the potential vorticity, which occurs by a decrease in layer thickness; hence as h approaches zero there is no further increase in transport. What happens in this case is the DWBC develops a vanishingly thin tail where the interface slope approaches the bottom slope (Fig. 7). This condition on interface slope is precisely what occurred in the large transport limit of the constant Q case. Note that it can only occur for the present case in such a vanishing tail where small changes in h (i.e. $h \approx$ constant) can still cause the required large changes in Q. Thus, interestingly the same maximum velocity occurs here as for the constant Q case (Fig. 7), and again the general rule applies that the DWBC interface slope cannot exceed the bottom slope. It is recognized that in such a thin onshore tail, bottom friction would surely become important. We present this large transport limit for instructional purposes only and note that all solutions considered in the present work are well below this limit and do not develop such a tail (consistent with our neglect of friction).

The importance of a varying potential vorticity distribution on the structure of the DWBC can be seen by comparing solutions for the constant Q current and analogous realistic Q current at northern latitudes (Fig. 8a). We now use a larger value of reduced gravity ($g' = .005$ m/s^2) as this highlights the difference between the two cases. At 55N the DWBC is in deep water so that the cross-stream change in Q can be accounted for by variation in h, so that $Q \approx f/h$. Thus the current is significantly wider with a correspondingly small relative vorticity ($v_x \approx 0$), precisely what we were looking for. Note that in this case v_x need not be less than or equal to zero everywhere, which leads to a smaller secondary peak on each shoulder of the current (Fig. 8a). As the current progresses southward to 35N, again the variation in h is sufficient to account for the change in Q, except at the very edges of the current (Fig. 8b). By 20N these edge regions of non-negligible shear extend a bit further into the current, but v_x is still substantially reduced from the constant Q case (not shown).

Eventually, the DWBC moves into shallow enough topography that the cross-stream change in h would cause Q to change too drastically, simply because h is

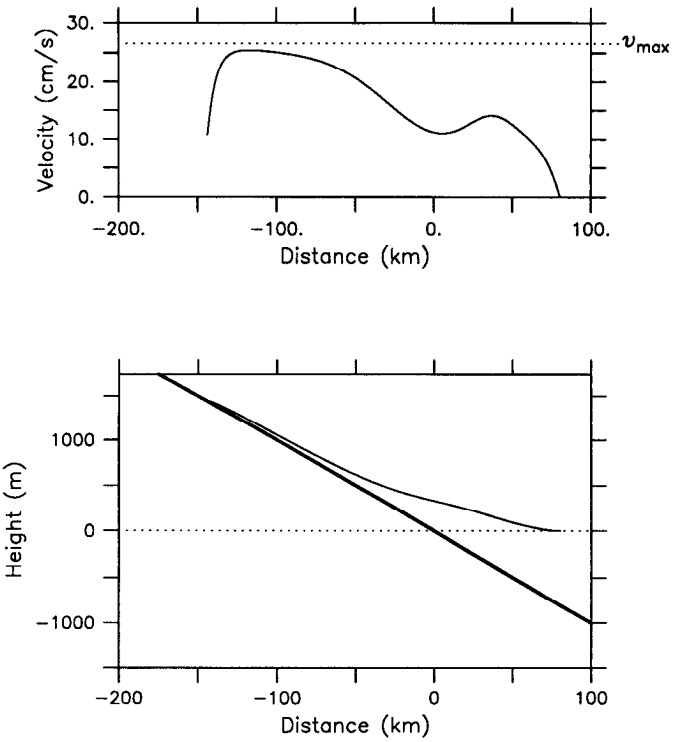

Figure 7. Large transport limit of the realistic Q DWBC. The upper panel shows the downstream velocity with the maximum possible value indicated. The lower panel is the interface. The parameters are $g' = .001$, $\alpha = .01$, latitude = 15N, Transport = 7.5 Sv.

already small. In this case the shear plays essentially the same role as in the uniform case; that is, it decreases significantly in response to the decreasing layer thickness onshore. This does not happen, however, until the southern limit of the domain (near 10N) where the constant Q and realistic Q solutions are in fact nearly comparable (Fig. 8c). The alongstream evolution of the realistic Q DWBC is summarized in Figure 9: over most of its path the current is substantially wider, weaker and reduced in shear—more characteristic of the observed DWBC.

5. Complex topography

In this section we consider a model with exponential bottom slope (as opposed to the linear slope in the previous sections), which is more representative of the actual continental slope. We also investigate how an inertial DWBC negotiates a ridge, in an effort to better understand how the North Atlantic DWBC flows around the Southeast Newfoundland Rise.

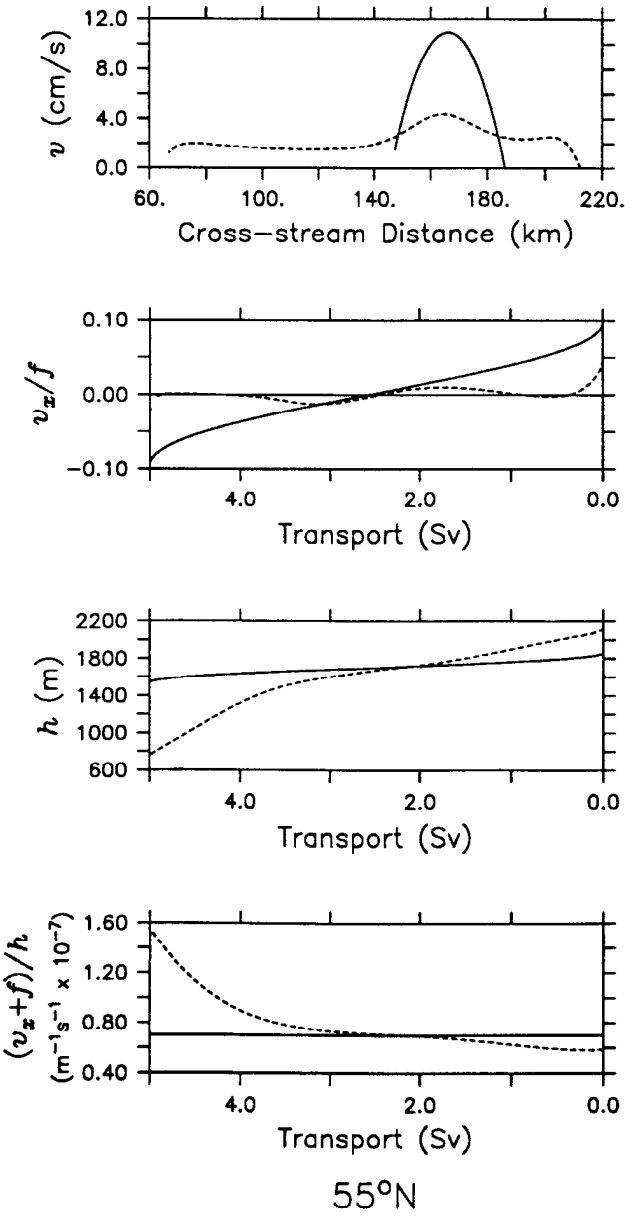

Figure 8. Cross-stream structure of the realistic Q DWBC (dashed-line) compared to the uniform Q solution (solid line). (a) Comparison at 55N. The top panel shows the downstream velocity; the second panel shows normalized relative vorticity and is plotted versus transport to facilitate the comparison; the third panel shows layer thickness; the bottom panel shows the corresponding distributions of potential vorticity. The parameters are $g' = .005$, $\alpha = .01$, Transport = 5 Sv. For the uniform potential vorticity current the value of Q is $.7\ m^{-1}s^{-1} \times 10^{-7}$. (b) Same comparison at 35N. (c) Same comparison at 10N.

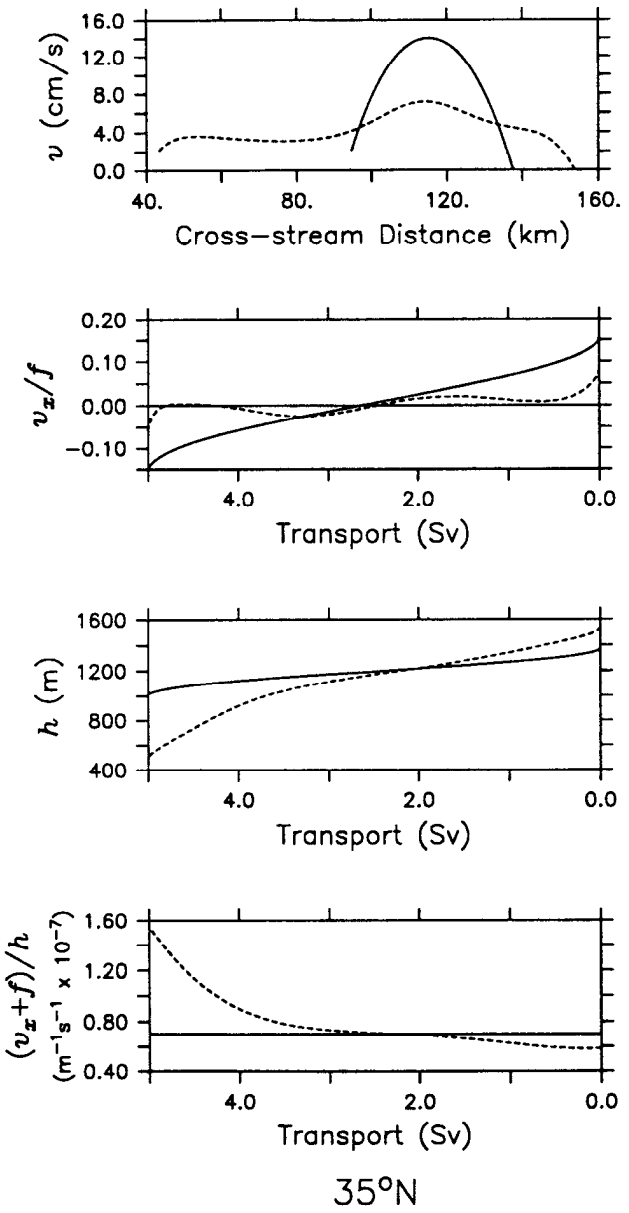

Figure 8. (Continued)

a. Exponential bottom slope. An exponential continental slope is of the form $b(x) = H_b[\exp(x/L_b) - 1]$, where L_b is the e-folding cross-stream length scale of the slope and H_b is the offshore layer thickness (Fig. 10); for the moment these are both assumed independent of latitude. Inserting this expression into Eq. (12) (which

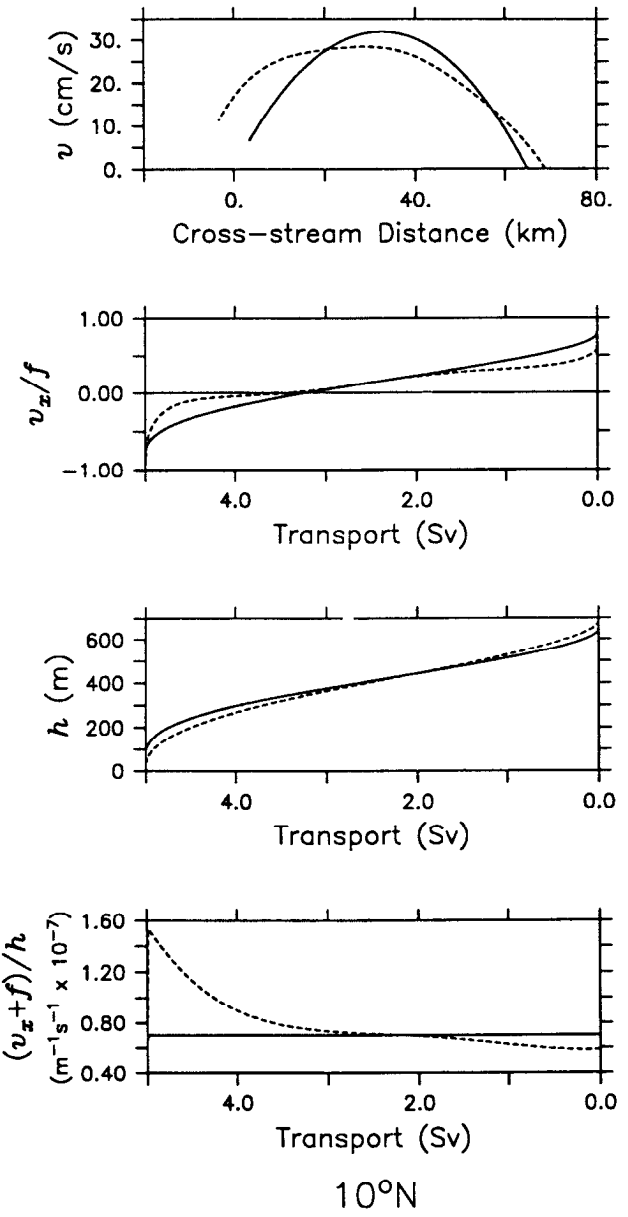

Figure 8. (Continued)

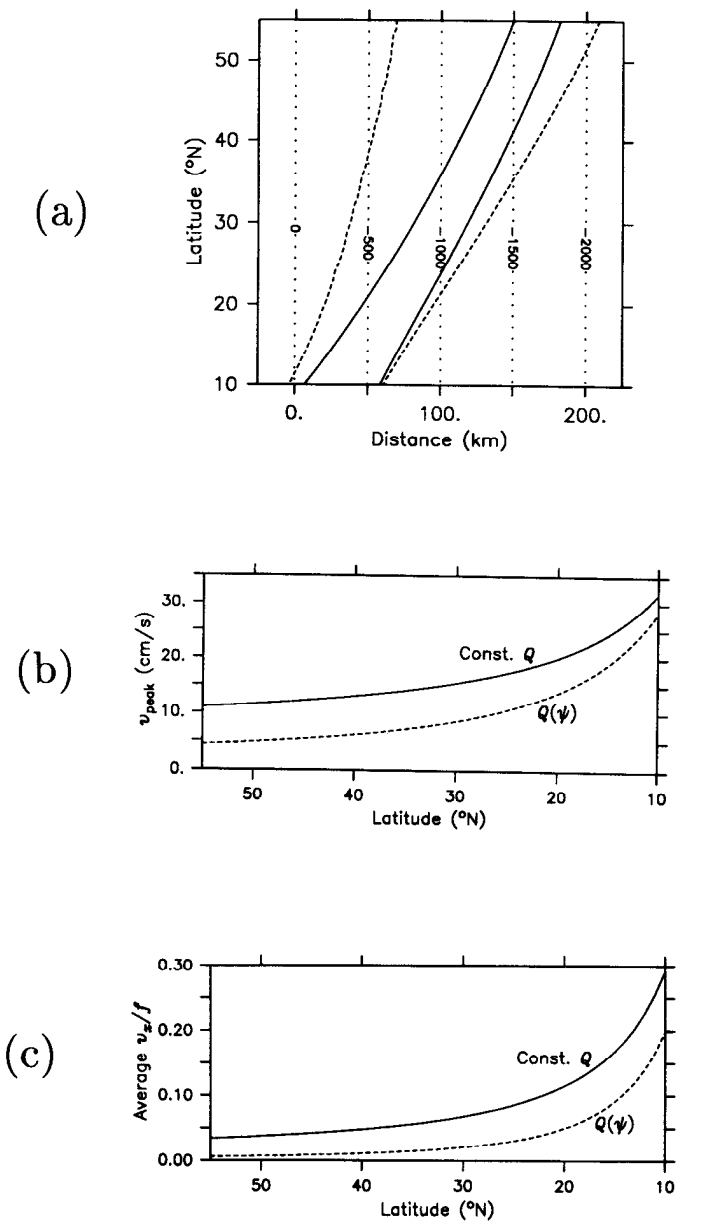

Figure 9. Alongstream evolution of the realistic Q DWBC (dashed lines) compared to the uniform Q current (solid lines). (a) Alongstream path of the current. (b) Peak velocity. (c) Normalized relative vorticity. The parameters are $g' = .005$, $\alpha = .01$, Transport = 5 Sv, $Q = 7\ m^{-1}s^{-1} \times 10^{-7}$ for the uniform potential vorticity current.

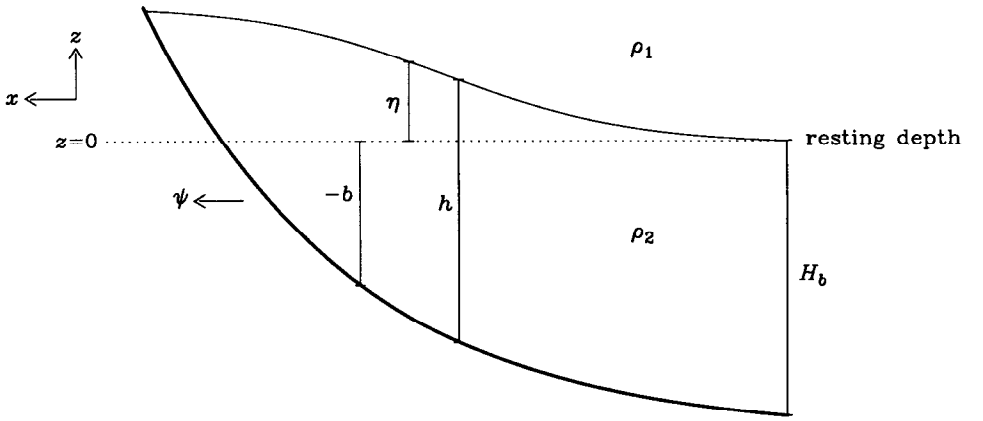

Figure 10. Schematic of the model with exponential bottom topography. The offshore layer thickness is H_b.

contains the bottom depth), and non-dimensionalizing with the earlier scales, gives the new Bernoulli equation for the uniform Q case,

$$\mathrm{h} = \psi - \frac{\epsilon}{2} v^2 - \frac{H_b}{H}(e^{s_b x} - 1), \tag{30}$$

where $s_b = L_c/L_b$. This, together with the remaining equations (17) and (19), are the new governing equations for the constant Q current. The only change in boundary conditions is that at the offshore edge of the current,

$$h = -\frac{H_b}{H}(e^{s_b x_o} - 1) \qquad \text{at } \psi = 0. \tag{31}$$

We find that as the transport of the current is increased, the interface slope increases accordingly but again cannot exceed the bottom slope. Thus the meridional velocity at each cross-stream point cannot exceed an upper limit $v_{\max}$, as shown in Figure 11. This can be compared to the linear bottom slope case (Fig. 3): in both instances the interface parallels the bottom (except at the edges) and h is constant. Note, however, that in the exponential case the shear v_x is not zero over this region, but equal to a small non-zero constant (6×10^{-7} s^{-1}, Fig. 11). This leads to an asymmetrical velocity profile and larger value of shear at the onshore edge which is characteristic of all solutions for the exponential bottom.

For the realistic Q boundary current there are also differences for an exponentially varying continental slope. The southward trajectory of the current changes its curvature such that it has the sense of being "funneled" by the increasing onshore bottom slope (Fig. 12). The current starts out wider at northern latitudes, then becomes thinner in the tropics. This is a reflection of the widening process analyzed by Stommel and Arons (1972) who showed that a weaker continental slope results in a wider DWBC. In the present case, when the DWBC is to the north in deeper water

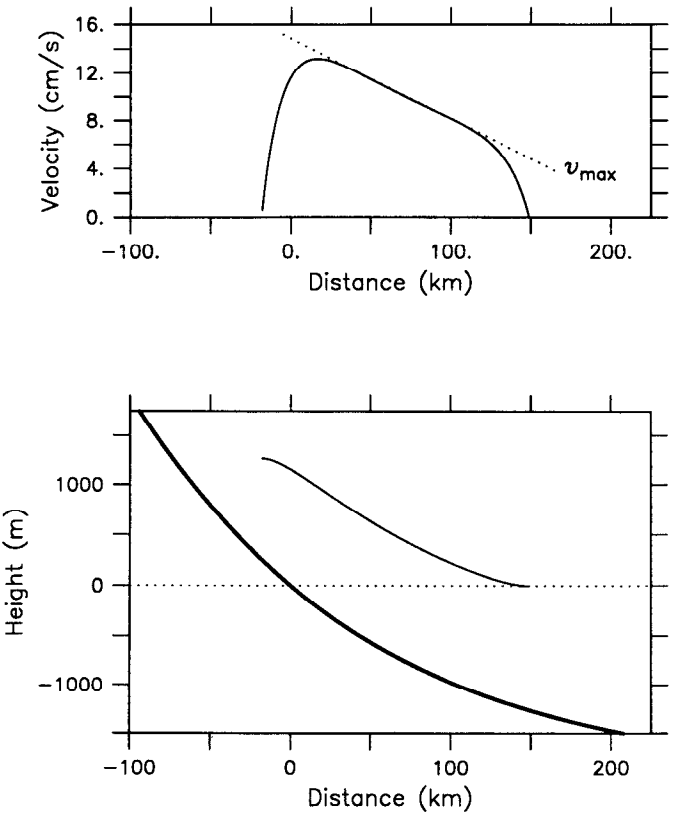

Figure 11. Large transport solution of the uniform Q current with an exponential bottom. The upper panel shows the downstream velocity with the maximum value indicated. The lower panel shows the interface. The parameters are $g' = .001$, $H_b = 2000$ m, $L_b = 150$ km, $Q = .7\ \mathrm{m^{-1}s^{-1}} \times 10^{-7}$, Transport = 18 Sv, latitude = 35N.

it experiences a locally weaker bottom slope, while to the south it resides over a much larger bottom slope. Recall that for the realistic Q DWBC the relative vorticity does not become significant until the southern limit of the domain, where the generally small layer thickness requires a substantial change in v_x to offset changes in h. The increased bottom slope (hence reduced layer thickness) upslope in the exponential case thus causes v_x to become significant at a more northerly latitude (Fig. 12), though it is still negligible over most of the current's length.

b. Topographic ridge. An important difference in the exponential bottom case is that the layer thickness eventually becomes constant offshore (versus the ever deepening

Figure 12. Path of the realistic Q DWBC for a linear bottom slope (upper panel) compared to an exponential continental slope (middle panel). The bottom panel compares the normalized relative vorticity for the two cases. The parameters are $g' = .005$, $\alpha = .01$, $H_b = 2000$ m, $L_b = 100$ km, Transport = 5 Sv.

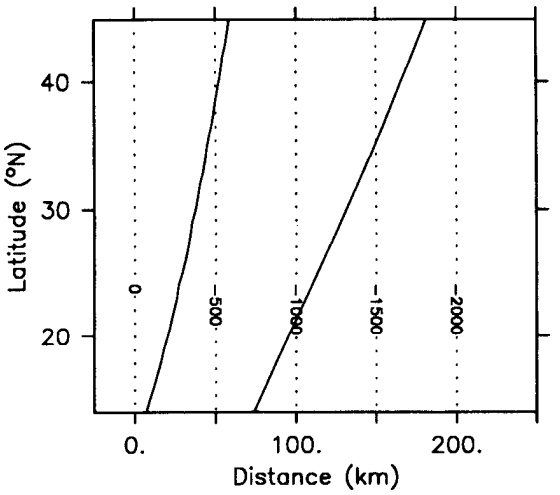
40
30
20
Latitude (°N)
0
500
1000
1500
2000
0.
100.
200.
Distance (km)

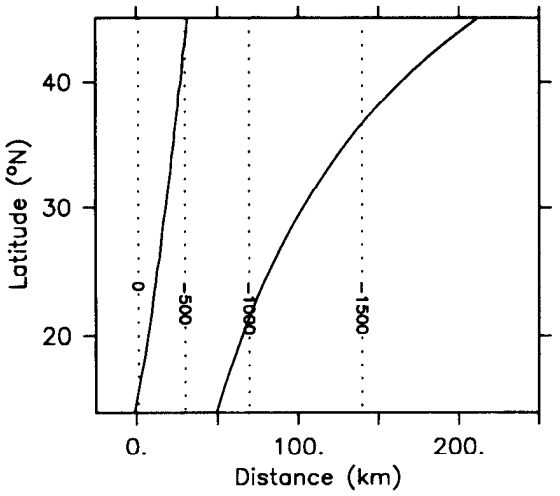
40
30
20
Latitude (°N)
0
500
1000
1500
0.
100.
200.
Distance (km)

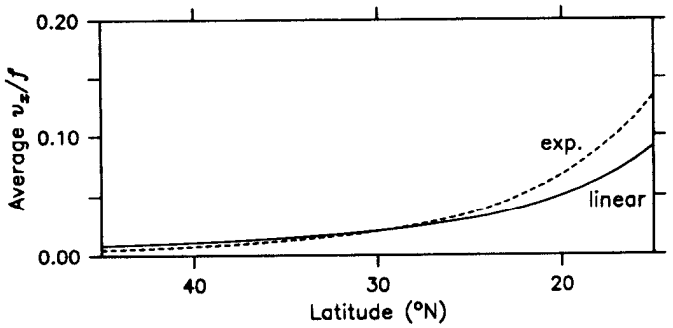
0.20
0.10
0.00
Average v_s/f
exp.
linear
40
30
20
Latitude (°N)

Figure 12

bottom in the linear slope case; compare Figs. 1 and 10). This is of course reflective of the actual continental slope. If the DWBC resides on this outer weak-portion of the slope there are important ramifications regarding the structure of the flow. Recall that at the offshore boundary of the DWBC the rhs of Eq. (17) (or Eq. (27) for the realistic Q case) must be positive for a southward flowing current. Dimensionally this implies that the initial layer thickness must be greater than $(f/f_o)H$ (or greater than f/A_0 for the realistic Q current, where in this section we take $f_o/H = A_0$ so in fact the condition is the same for both currents). Satisfying this condition is not a problem for a linear sloping bottom; recall that the offshore edge of the current x_o must simply be far enough seaward to obtain a sufficiently large initial layer thickness. However, in the exponential case the layer thickness is now bounded offshore so in fact the bottom could be shallow enough that this condition would not be satisfied. As explained below, in this case a full solution is not possible. Thus, there is now an additional criterion on the topography for a complete southward flowing DWBC: $H_b > (f/f_o)H$.

In the present model we envision that the potential vorticity of the current is set at an upstream location (say shortly beyond the overflow) where the topography satisfies this condition. Allowing now the bathymetry to vary with y, one could envision that further downstream the current encounters a topographic ridge (i.e. smaller H_b) which is shallow enough that the condition is violated. In this case the ridge represents a potential vorticity barrier. Such "blocking" is akin to that discussed by Nof (1980) for the simpler case of a barotropic current encountering topography which is independent of cross-stream position. Prior to the critical value of H_b (i.e. for a ridge slightly deeper than this) the full current can progress past the ridge but its local structure is significantly altered. For the constant Q case, the current broadens significantly at the sill (Fig. 13a) as the interface nearly parallels the bottom (Fig. 14, solid line); the current's constant potential vorticity is satisfied by a nearly uniform h which implies negligible shear (hence the weak velocity and large width). For deeper ridges this effect is reduced because the current can reside farther up the slope (i.e. it extends only partially onto the ridge).

For a ridge which is taller than the critical value, a solution can only exist if the offshore interface height remains higher than the original (upstream) resting depth (Fig. 14, dashed line). This is a valid solution, but note that it does not account for the full transport of the current. The new offshore interface level can be thought of as an "intermediate" resting level, where the remainder of the transport is forced to flow along the ridge (Fig. 13b); north of this outer part of the ridge the interface drops to the original resting level. Eventually this portion of the current (which we do not explicitly solve for) either recirculates or flows around the end of the ridge.

In order to obtain the partial transport solution at the ridge when the ridge is taller than the critical value, it is necessary to solve the system of Eqs. (17)–(19) (or (27)–(29) for the realistic Q case) from the opposite direction, i.e. progressing

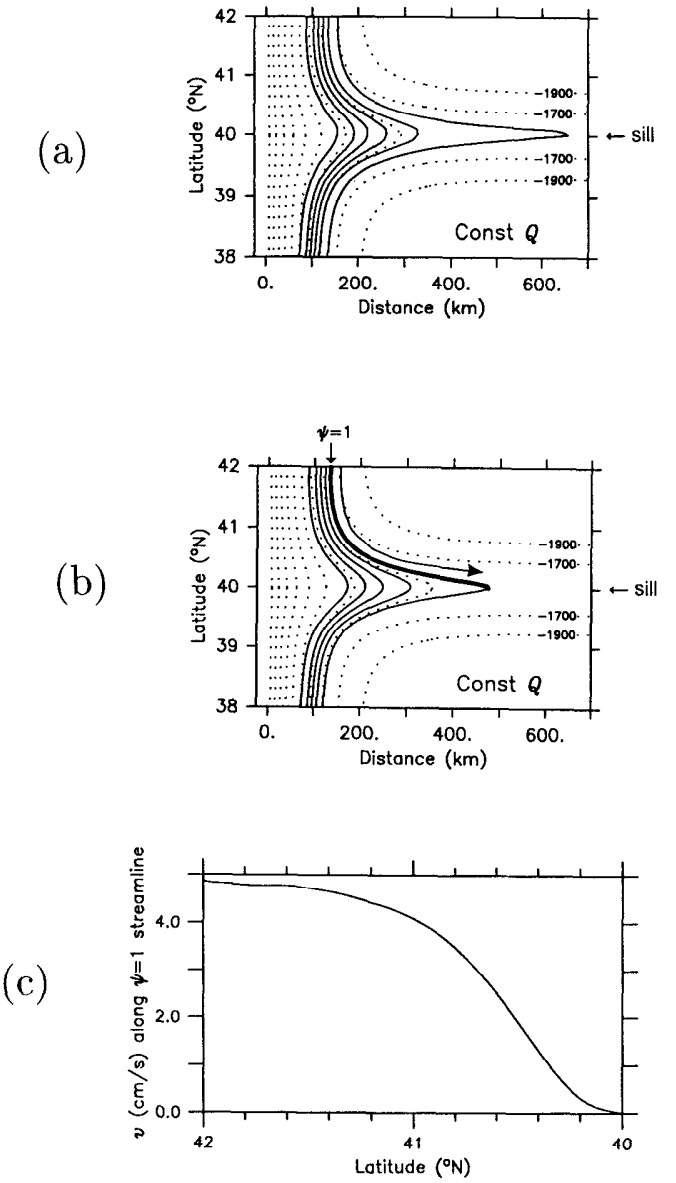

Figure 13. Streamlines (ψ = 0–5 Sv) of the uniform Q DWBC negotiating two different ridges, one on either side of the critical limit (see text). The topography is indicated by the dotted lines. The parameters are $g' = .001$, $Q = .5862\ \mathrm{m^{-1}s^{-1}} \times 10^{-7}$. (a) The deeper ridge which allows the full current to pass. (b) The higher ridge which blocks 1 Sv. The arrow signifies that the diverted transport continues eastward. (c) Downstream velocity along the bold portion of the $\psi = 1$ streamline in (b). To the south of the sill the velocity remains identically zero along this streamline.

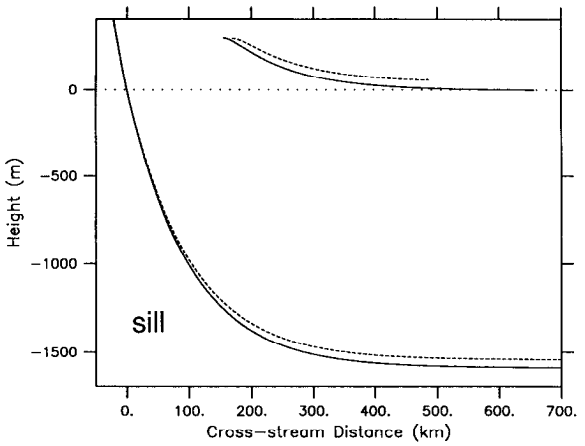

Figure 14. Vertical section at the sill in Figure 13a and b. The solid line corresponds to the ridge in Figure 13a which is just deep enough to permit the full transport solution (5 Sv); the dashed line is for the higher ridge of Figure 13b which causes partial blocking (allows 4 Sv).

onshore to offshore. This is because we do not know beforehand what the offshore value of ψ will be (which depends on the height of the ridge). The solution is thus initiated from the onshore boundary where $\psi = \psi_{max}$ (designated transport of the current) and $v = 0$. Using the shooting method as before, we guess an initial value of x_w (the onshore edge of the current), and use the Bernoulli function to obtain the corresponding value of h at this boundary. Then the solution is determined as v decreases back to zero, at which point $\psi = \psi_{min} > 0$ (i.e. the transport of this solution, $\psi_{max} - \psi_{min}$, is less than the full designated transport). We then revise x_w and iterate, until the limiting value is determined which gives the smallest ψ_{min}. This solution represents the maximum transport permitted to flow equatorward by the given ridge height. As the ridge is made taller, more of the transport is diverted outward along the ridge as the offshore interface height must be even higher. Eventually the entire current can be blocked.

In the example of Figure 13b, 1 Sv is diverted along the ridge (i.e. the flow between the $\psi = 0$ and $\psi = 1$ streamlines). Thus, south of the sill the $\psi = 1$ contour represents the offshore edge of the current, along which $v = 0$ (which is the boundary condition). This means that as the sill is approached the velocity along the $\psi = 1$ streamline must go to zero. This is verified in Figure 13c which plots the velocity along the bold portion of the $\psi = 1$ streamline in Figure 13b: the velocity indeed decreases smoothly to zero toward the sill. Note that in the separated flow $v = 0$ as well, which is consistent with the application of the Bernoulli function ($B = v^2/2 + g'(h + b)$) at the bifurcation point.

It is recognized that the semi-geostrophic assumption will be formally violated as v approaches zero near the sill of the ridge. This can be checked by computing the cross-stream velocity u from the y-momentum equation, and determining the ratio

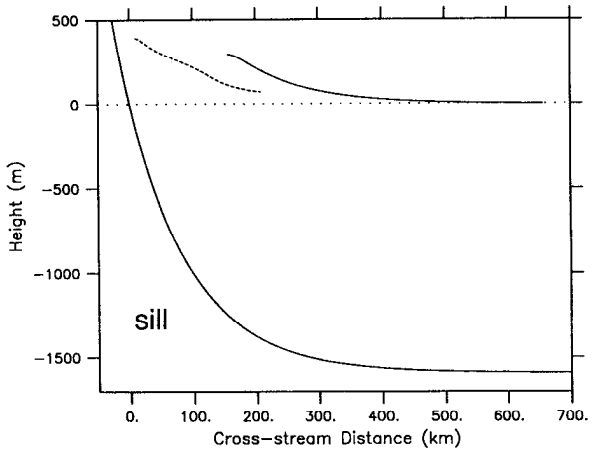

Figure 15. Interface of the uniform Q current over the deeper ridge of Figure 13a (solid line) compared with the interface of the realistic Q current over the same ridge (dashed line). The realistic Q current is partially blocked (allows 3.8 Sv).

$|u_y|/|v_x|$, which should be less than one for semi-geostrophy. In the present case, near the sill u_y is in fact larger than v_x. However, we are interested only in demonstrating that potential vorticity blocking can occur, and are not concerned about the precise detail of the offshore-most flow. As a test we considered successively broader ridges (thereby reducing the y-variation in the problem). The above ratio is reduced accordingly, and can be made as small as 1 ($v_x \sim u_y$). In each case the amount of recirculation remains the same, suggesting that inclusion of the inertial terms in the x-momentum equation would not in fact alter the basic result.

For the realistic potential vorticity DWBC, ridges can have an even more significant dynamical impact. The reason for this can be seen in the previous example (Fig. 14, solid line), where a ridge just below the critical height causes a nearly uniform DWBC layer thickness. In the realistic Q case the potential vorticity varies across the current, thus such a solution would not be allowable (and recall that the interface cannot slope more steeply than the bottom so the shear would not be able to compensate). Thus a ridge which is deep enough to permit the entire uniform Q DWBC does not necessarily allow the full realistic Q DWBC.

This situation can be investigated using the method of solution described above, i.e. solving the equations in the offshore direction. As before, there is a critical ridge height (deeper than the critical height for the uniform Q current) above which a full solution is not possible. Again, the outer portion of the current is truncated (and flows along the ridge). The remaining flow is situated further onshore over steeper topography, which allows for the necessary cross-stream variation in layer thickness (hence Q) associated with the realistic Q current (Fig. 15). Note then that the partial transport solution in this case is allowed past the ridge for a different reason than in

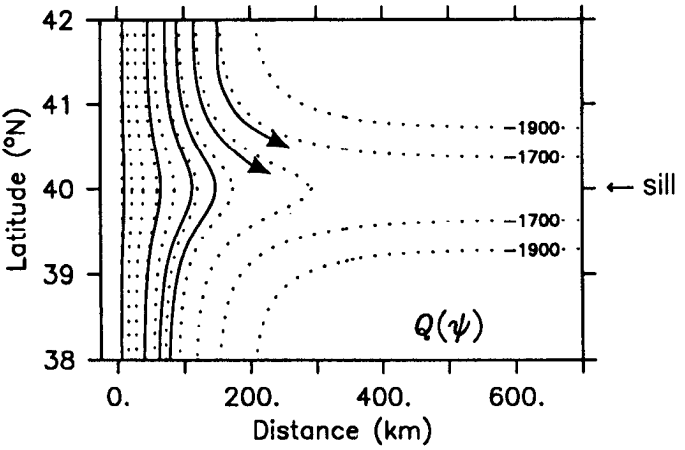

Figure 16. Streamlines (ψ = 0–5 Sv) of the realistic Q current negotiating the deeper ridge of Figure 13a, which blocks 1.2 Sv.

the constant Q case: in the former it is because the offshore layer thickness becomes large enough, while in the present case it is because the variation in layer thickness becomes large enough. This phenomenon is demonstrated in Figure 16, where the same ridge which allowed the full constant Q current is seen to block a portion of the realistic Q current. As the ridge becomes even higher it will eventually impact the realistic Q current for both reasons stated above.

Thus, a topographic ridge can more easily act as a barrier for a current with cross-stream variation in potential vorticity—variation which is indicative of the North Atlantic DWBC. Such potential vorticity blocking may in fact be at work at the Southeast Newfoundland Rise where the DWBC attempts to flow around the Grand Banks. Two recent hydrographic sections occupied on either side of the ridge indicate that the deepest part of the DWBC does not progress past the ridge (Fig. 17). It is seen that water of high oxygen concentration (indicative of recent ventilation) deeper than 3500 m is present at the upstream section but not at the downstream section. This recirculation has been noted previously (e.g. Clarke, 1993).

Finally, recall that near the southern limit of the model domain the realistic Q solution approaches that of the uniform Q current. Thus, in the tropics a ridge will act the same on both types of currents. This means that ridges are more of a dynamical barrier at more northerly latitudes. This is documented in Figure 18 which shows how much deeper a ridge must be to permit a full realistic Q DWBC (versus a constant Q DWBC). At 15N the difference is negligible, while north of 60N the ridge must be over 500 m deeper. This suggests that if a feature such as the Southeast Newfoundland Rise were located at low latitudes, it would not necessarily lead to recirculation.

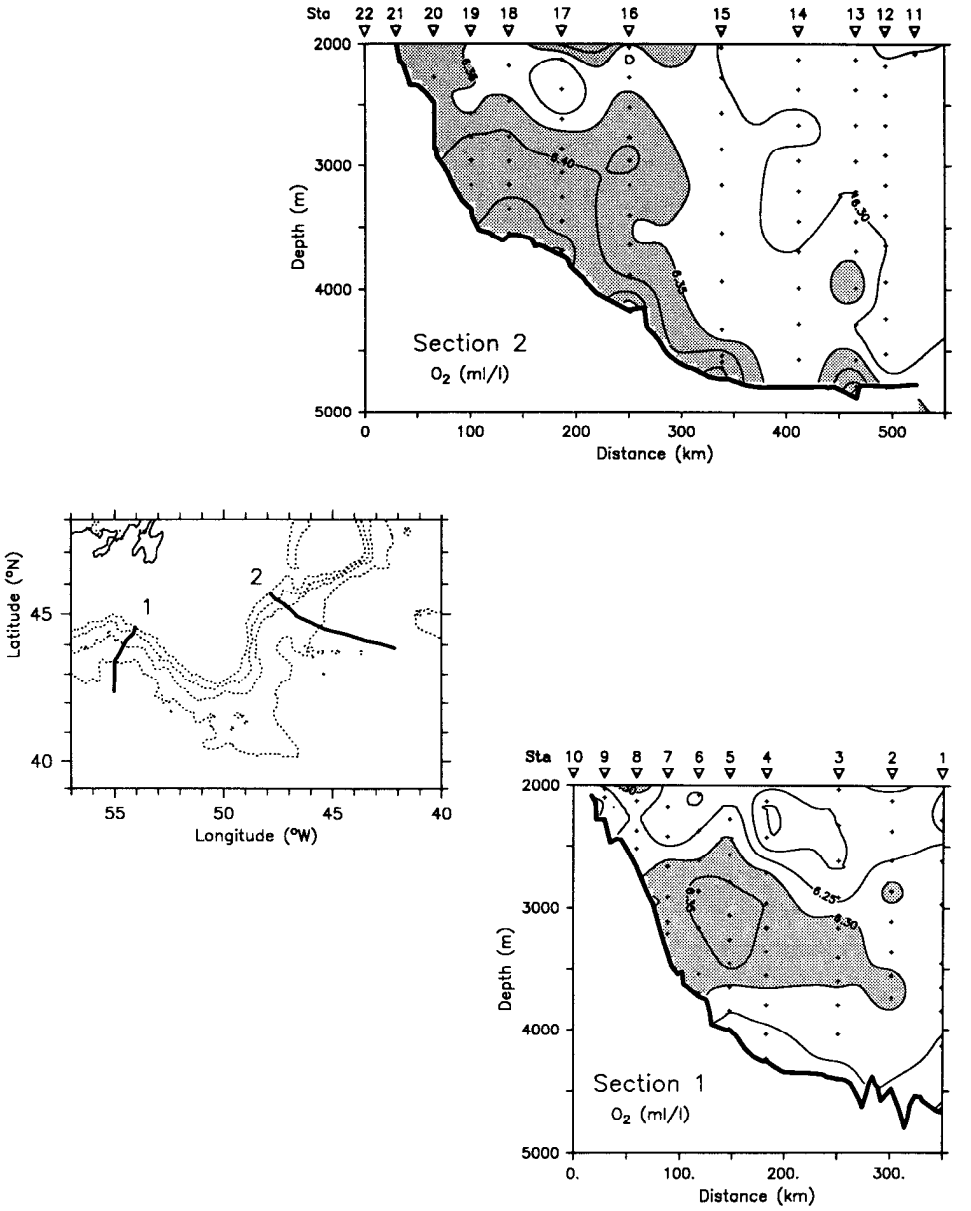

Figure 17. Two oxygen sections on either side of the Southeast Newfoundland Rise, as indicated on the lateral bathymetry map (from McKee *et al.* (1994)). The shaded region is the high oxygen Norwegian-Greenland overflow water of the North Atlantic DWBC.

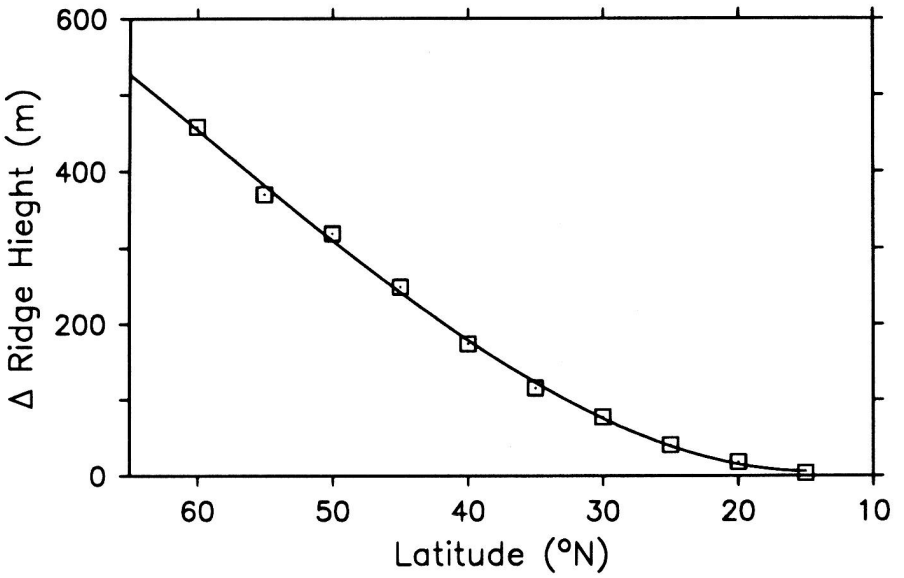

Figure 18. Difference in blocking ridge height for a uniform Q versus realistic Q current as a function of latitude (i.e. the ridge must be this much deeper to permit the entire realistic Q current). The model parameters are $g' = .001$, Transport = 5 Sv, $Q = .5862\ m^{-1}s^{-1} \times 10^{-7}$ for the uniform potential vorticity current.

6. Summary

A steady, inertial model of the DWBC has been developed which incorporates a realistic cross-stream distribution of potential vorticity (Q), calculated from a hydrographic section across the North Atlantic DWBC at 35N. The model is a reduced gravity semigeostrophic current on a continental slope, and is solved using the transport streamfunction as the independent variable. A general result is that the interface slope of the DWBC cannot exceed the local bottom slope, and in the limit of large transport it parallels the bottom. The tendency for this to happen increases at higher latitudes.

The structure of the realistic Q current was compared to that of a uniform potential vorticity current investigated in previous studies. When the potential vorticity increases across-stream as the data indicate, this enables variation in the model layer thickness without compensating variation in relative vorticity. This means that over the interior of the current the relative vorticity is vastly reduced from the uniform case, resulting in a wider, weaker DWBC which is more in line with observations. This holds true until the current reaches the tropics at which point the realistic Q current approaches the uniform potential vorticity solution.

When the continental slope varies exponentially (more in line with the actual continental slope) the general tendencies of the realistic Q current remain the same. The current is, however, somewhat wider at northern latitudes because it is located

on the outer (weaker) part of the slope. The manner in which an inertial DWBC negotiates a ridge was investigated using the exponential topography. There is a critical ridge height above which the offshore portion of the current is blocked and must flow eastward along the ride. Furthermore, while a ridge which is deeper than this critical height will permit the entire uniform Q current to pass, it may still block a portion of the realistic Q current. This is because the flat portion of the ridge causes a weak interface slope which results in a nearly uniform layer thickness, a condition which cannot be attained in the realistic Q current. Such a bifurcation may explain the observed splitting of the DWBC at the Southeast Newfoundland Rise.

Acknowledgments. The authors acknowledge A. Gangopadhyay and T. McKee for their help in calculating the reduced gravity using the hydrographic data. R. Pickart was supported by NSF grant OCE90-18409; R. Huang was supported by NSF grant OCE93-00706 and NOAA grant NA36GP0270. This is WHOI contribution number 8681.

REFERENCES

Clark, R. A. 1993. The North Atlantic Current in the Northwest Atlantic, *in* The North Atlantic Current System: A Scientific Report. Proceedings from the North Atlantic Current Workshop at the Woods Hole Oceanographic Institution, P. Rizzoli and T. Rossby, eds., 132 pp.

Grant, A. B. 1968. Atlas of Oceanographic Sections, Temperature-Salinity-Dissolved Oxygen-Silica, Davis Strait-Labrador Basin-Denmark Strait-Newfoundland Basin, 1965–1967. Rep. A.O.L. 68-5, Atlantic Oceanographic Laboratory, Bedford Institute, Dartmouth, N.S., Canada.

Griffiths, R. W., P. D. Killworth and M. E. Stern. 1982. Ageostrophic instability of ocean currents. J. Fluid Mech., *117,* 343–377.

Johns, W. E., D. M. Fratantoni and R. J. Zantopp. 1993. Deep western boundary current variability off northeastern Brazil. Deep-Sea Res., *40,* 293–310.

Johnson, G. C. 1993. A deep inertial jet on a sloping bottom near the equator. Deep-Sea Res., *40,* 1781–1792.

Kawase, M. 1993. Topographic effects on the bottom water circulation of the western tropical North Atlantic Ocean. Deep-Sea Res., *40,* 1259–1283.

Kawase, M. and D. Straub. 1991. Spinup of source-driven circulation in an abyssal basin in the presence of bottom topography. J. Phys. Oceanogr., *21,* 1501–1514.

Killworth, P. D. 1993. On the role of dissipation in inertial western boundary currents. J. Phys. Oceanogr., *23,* 539–553.

MacCready, P. 1993. Frictional decay of the deep western boundary current in the northern North Atlantic. J. Mar. Res., *52,* 197–217.

McKee, T. K., R. S. Pickart and W. M. Smethie, Jr. 1994. Hydrographic data report for *Endeavor* 223. WHOI Data Report.

Nof, D. 1980. The influence of varying bathymetry on inertial boundary currents. Tellus, *32,* 284–295.

Nof, D. and D. B. Olson. 1993. How do western abyssal currents cross the equator? Deep-Sea Res., *40,* 235–255.

Pedlosky, J. and D. C. Chapman. 1993. Baroclinic structure of the abyssal circulation and the role of meridional topography. J. Phys. Oceanogr., *23,* 979–991.

Pickart, R. S. 1992. Space-time variability of the Deep Western Boundary Current oxygen core. J. Phys. Oceanogr., *22,* 1047–1061.

Pickart, R. S. and N. G. Hogg. 1989. A tracer study of the deep Gulf Stream cyclonic recirculation. Deep-Sea Res., *36,* 935–956.

Pickart, Robert S. and William M. Smethie, Jr. 1993. How does the Deep Western Boundary Current cross the Gulf Stream? J. Phys. Oceanogr, *23,* 2602–2616..

Smith, P. C. 1975. A streamtube model for bottom boundary currents in the ocean. Deep-Sea Res., *22,* 853–873.

Spall, M. A. 1994. Wave-induced abyssal recirculations. J. Mar. Res., *52,* 1051–1080.

Speer, K. and E. Tziperman. 1990. Convection from a source in an ocean basin. Deep-Sea Res., *37,* 431–446.

Stommel, H. and A. B. Arons. 1972. On the abyssal circulation of the world ocean—V. The influence of bottom slope on the broadening of inertial boundary currents. Deep-Sea Res., *19,* 707–718.

Straub, D. N., P. D. Killworth and M. Kawase. 1993. A simple model of mass-driven abyssal circulation over a general bottom topography. J. Phys. Oceanogr., *23,* 1454–1469.

Warren, B. A. 1976. Structure of deep western boundary current. Deep-Sea Res., *23,* 129–142.

Received: *24 March, 1994;* revised: *25 April, 1995.*